Springer Theses
Recognizing Outstanding Ph.D. Research

Mika Vesterinen

Z Boson Transverse Momentum Distribution, and ZZ and WZ Production

Measurements Using 7.3 – 8.6 fb^{-1} of $p\bar{p}$ Collisions at $\sqrt{s} = 1.96$ TeV

Springer

Springer Theses

Recognizing Outstanding Ph.D. Research

For further volumes:
http://www.springer.com/series/8790

Aims and Scope

The series "Springer Theses" brings together a selection of the very best Ph.D. theses from around the world and across the physical sciences. Nominated and endorsed by two recognized specialists, each published volume has been selected for its scientific excellence and the high impact of its contents for the pertinent field of research. For greater accessibility to non-specialists, the published versions include an extended introduction, as well as a foreword by the student's supervisor explaining the special relevance of the work for the field. As a whole, the series will provide a valuable resource both for newcomers to the research fields described, and for other scientists seeking detailed background information on special questions. Finally, it provides an accredited documentation of the valuable contributions made by today's younger generation of scientists.

Theses are accepted into the series by invited nomination only and must fulfill all of the following criteria

- They must be written in good English.
- The topic should fall within the confines of Chemistry, Physics, Earth Sciences, Engineering and related interdisciplinary fields such as Materials, Nanoscience, Chemical Engineering, Complex Systems and Biophysics.
- The work reported in the thesis must represent a significant scientific advance.
- If the thesis includes previously published material, permission to reproduce this must be gained from the respective copyright holder.
- They must have been examined and passed during the 12 months prior to nomination.
- Each thesis should include a foreword by the supervisor outlining the significance of its content.
- The theses should have a clearly defined structure including an introduction accessible to scientists not expert in that particular field.

Mika Vesterinen

Z Boson Transverse Momentum Distribution, and ZZ and WZ Production

Measurements Using 7.3–8.6 fb^{-1} of $p\bar{p}$ Collisions at $\sqrt{s}$ = 1.96 TeV

Doctoral Thesis accepted by
the University of Manchester, UK

Springer

Author
Dr. Mika Vesterinen
University of Manchester
United Kingdom

Supervisor
Prof. Terry Wyatt
University of Manchester
United Kingdom

ISSN 2190-5053 ISSN 2190-5061 (electronic)
ISBN 978-3-642-30787-4 ISBN 978-3-642-30788-1 (eBook)
DOI 10.1007/978-3-642-30788-1
Springer Heidelberg New York Dordrecht London

Library of Congress Control Number: 2012940240

Printed on acid-free paper

Springer is part of Springer Science+Business Media (www.springer.com)

Supervisor's Foreword

This Ph.D. thesis presents three major pieces of new work:

- the development of novel techniques for measuring the transverse momentum of Z bosons;
- the application of these novel techniques to data from the DØ experiment at the Tevatron and a comparison of the measured distributions with state-of-the-art QCD calculations;
- precise measurements of the cross sections for WZ and ZZ vector boson pair production [1].

A novel analysis variable, ϕ^*_η, is proposed [2]. This is sensitive to the same physics as the $p_T^{\ell\ell}$ distribution, but is significantly less susceptible to the effects of detector resolution and efficiency. In particular, since ϕ^*_η depends exclusively on the directions of the two leptons, which are measured with a precision of a milliradian or better, ϕ^*_η is experimentally very well measured compared to any quantities that rely on the momenta of the leptons.

Using 7.3 fb^{-1} of $p\bar{p}$ collisions collected by the DØ detector at the Fermilab Tevatron, the normalized cross section is measured as a function of the variable ϕ^*_η in bins of boson rapidity and in both dielectron and dimuon final states [3]. These measurements are of unprecedented precision and expose deficiencies in the current state-of-the-art QCD predictions for vector boson production at hadron colliders. In addition, these data exclude in hadron–hadron collisions the hypothesis of 'low-x broadening' (This is the idea that the intrinsic transverse momentum of partons inside the proton becomes broader as the momentum fraction x becomes very small).

These new experimental techniques and measurements have stimulated considerable interest in the theoretical and experimental particle physics communities. For example, resummed QCD calculations of the distribution of ϕ^*_η have been made and compared with the above DØ measurements [4]. Measurements of ϕ^*_η are now being extended at the Tevatron to lepton pairs with masses outside the Z

resonance region. These techniques have now been picked up by the LHC experiments, where measurements of ϕ_η^* distributions are now being performed.

The measurements of the cross sections for *WZ* and *ZZ* vector boson pair production build on earlier measurements by DØ, but use improved analysis techniques and almost the full Tevatron Run II data set. At the time of their publication [1] they represent the world's most precise measurements of the cross sections for *WZ* and *ZZ* production. These cross sections are sensitive to anomalous triple-gauge-couplings, and thus probe the electroweak component of the standard model. *WZ* and *ZZ* production are two of the smallest cross section processes currently accessible at a hadron collider and represent major sources of background in search channels for Higgs bosons. Understanding these processes is therefore crucial for demonstrating sensitivity to the presence of a standard model Higgs boson at the Tevatron.

Manchester, April 2012 Prof. Terry Wyatt

References

1. DØ Collaboration, V. M. Abazov et al., arXiv:1201.5652v1 [hep-ex] (2012) [submitted to Phys. Rev. D]
2. A. Banfi, S. Redford, M. Vesterinen, P. Waller, T.R. Wyatt, Eur. Phys. J. C **71**, 1600 (2011)
3. DØ Collaboration, V. M. Abazov et al., Phys. Rev. Lett. **106**, 122001 (2011).
4. A. Banfi, M. Dasgupta, S. Marzani, L. Tomlinson, High Energy Phys. **1201**, 044 (2011)

Acknowledgments

First of all I would like to thank my Supervisor, Terry Wyatt, for guiding me through the past 4 years with endless enthusiasm and ingenuity.

Thanks to Fred Loebinger for inspiring me to apply to this program (and also to the MPhys program 4 years earlier), and to Stefan Söldner-Rembold for encouraging me to join the D0 experiment. I am grateful for the tireless IT support (and entertainment) from Sabah Salih while based in Manchester. I would like to thank Mark Owen for helping me to get started with the various D0 frameworks and general coding during my first year. Thanks to all members of the D0 Manchester group and other friends who helped to make my 2 years at Fermilab enjoyable.

Of course I am thankful that my fiancée Joanna Burgess has been so patient and understanding during the last 4 years; particularly the 2 years that I was based at Fermilab. I also thank my parents for always supporting my apparent interest in science from an early age.

Contents

Chapter 1
Introduction and Theoretical Background

This thesis documents two analyses performed with the large sample of dielectron and dimuon events collected by the D0 detector at the Fermilab Tevatron. The first analysis takes a novel approach to the long studied Drell-Yan transverse momentum distribution, which probes higher order effects in Quantum chromodynamics. The second analysis studies the production of ZZ and WZ in final states with charged leptons and missing transverse momentum.

This chapter introduces the Standard Model of particle physics, and motivates the analyses presented in this thesis. Chapter 2 details the main components of the Tevatron accelerator chain, and the D0 detector. Chapter 3 describes some of the experimental techniques used to reconstruct and identify particles, and to measure their energies/momenta. In Chap. 4, detailed calibrations of electron and photon energies are developed for poorly instrumented regions of the calorimeter. Chapter 5 introduces several novel variables for studying the Drell-Yan transverse momentum distribution. Chapter 6 documents a measurement of the Drell-Yan cross section as a function of one of these variables, ϕ_η^*. Chapter 7 documents a measurement of the ZZ and WZ production cross sections. Finally, Chap. 8 presents the conclusions drawn from the work in this thesis.

1.1 The Standard Model

The Standard Model (SM) of particle physics has been extremely successful in describing the interactions of high energy particles, up to the energies that have been probed by experiments so far—roughly one TeV. This theory was largely based on the work of Glashow [1], Weinberg [2] and Salam [3], and earned them the 1979 Nobel prize.

Matter is understood in terms of twelve elementary spin-$\frac{1}{2}$ fermions (the quarks and leptons), as listed in Table 1.1, with each having an anti-matter equivalent. Interactions between these fermions are mediated by the spin-1 vector bosons; the photon (γ) of the electromagnetic force, the $W^\pm$ and Z bosons of the weak force, and the

M. Vesterinen, *Z Boson Transverse Momentum Distribution, and ZZ and WZ Production*, Springer Theses, DOI: 10.1007/978-3-642-30788-1_1,

Table 1.1 The elementary particles in the SM, all of which have been observed experimentally except for the Higgs boson

Fermions				Bosons
Quarks:	$\begin{pmatrix} u \\ d \end{pmatrix}$	$\begin{pmatrix} c \\ s \end{pmatrix}$	$\begin{pmatrix} t \\ b \end{pmatrix}$	γ, $W^{\pm}$, Z, g
Leptons:	$\begin{pmatrix} e \\ \nu_e \end{pmatrix}$	$\begin{pmatrix} \mu \\ \nu_\mu \end{pmatrix}$	$\begin{pmatrix} \tau \\ \nu_\tau \end{pmatrix}$	H

gluon (g) of the strong force. Certain interactions between the bosons themselves are also predicted. An additional spin-0 scalar Higgs field (H) provides a mechanism to give masses to the weak bosons, whilst allowing the photon to remain massless. The Higgs field also provides masses for the fermions. Apart from the Higgs, all of these particles have been observed experimentally. A quantum theory that includes gravity remains a theoretical dream for now.

Much of this structure results from requiring that the SM Lagrangian is invariant under *local gauge transformations*, $\psi \rightarrow \psi e^{i\phi(x)}$, where *local* specifies that the phase ϕ depends on the space-time coordinates x. This condition requires the existence of the gauge bosons and their interactions with the fermions. The interactions of the SM particles are described by the set of gauge groups

$$SU(3)_C \otimes SU(2)_L \otimes U(1)_Y,$$

where $SU(3)_C$, $SU(2)_L$ and $U(1)_Y$ are the gauge groups of colour, weak isospin, and weak hypercharge respectively. Each of these gauge groups will be described in more detail in the sections to follow.

Despite the remarkable success of the SM (we shall see results of some of the most stringent experimental tests in Sect. 1.3), it is still assumed to be a low energy effective theory. Firstly, the SM does not contain a natural candidate for the dark matter required by observations in astrophysics. Secondly, the SM is unable to account for the matter anti-matter asymmetry of the universe. Thirdly, the Higgs boson mass would acquire large loop corrections from whatever physics lies between the Electroweak scale and the Plank scale.[1] A popular extension to the SM that attempts to solve the problems mentioned above is Supersymmetry, where each SM particle has a superpartner with a different spin. Fermions have scalar (sfermion) superparters and bosons have fermion (gaugino) superpartners. Reference [4] provides an excellent overview of Supersymmetry. An alternative is to introduce extra dimensions through which gravity is allowed to propagate, but confining the SM particles to a 4D "brane" [5].

[1] At the Plank scale quantum effects on gravity become significant. The Plank scale is defined as $\Lambda_{\text{Plank}} = (8\pi G_N)^{-1/2} \approx 10^{19}$ GeV, where G_N is the gravitational constant.

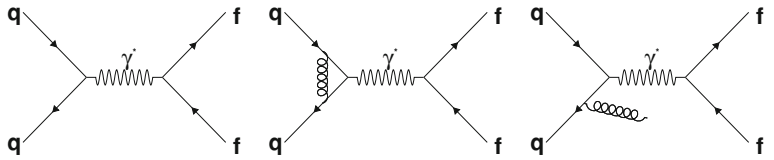

Fig. 1.1 *Left* tree level Feynman diagrams for quark anti-quark annihilation to a pair of fermions through a virtual photon. *Centre* similar diagram with a virtual gluon exchange between the incoming quark and anti-quark. *Right* similar diagram with a real gluon emission off one of the quarks

1.2 Scattering Amplitudes

In the limit that the relevant coupling constants are small (the perturbative regime), cross sections for particle interactions can be calculated using the method of Feynman diagrams. Figure 1.1 (left subfigure) shows a Feynman diagram for the annihilation of a quark and antiquark into a pair of fermions via the exchange of a virtual photon. A quantum mechanical amplitude for such a diagram is calculated by assigning a multiplicative factor for each line and vertex. Figure 1.1 also shows two (of the many) additional diagrams which appear at higher orders in Quantum chromodynamics, which will be described in Sect. 1.4. The central diagram includes a *virtual* or loop correction, and the right hand diagram includes a *real* or radiative correction. The accuracy of cross section calculations depends on the order of diagrams considered. Typically, the coupling constant associated with higher order corrections is small enough that the problem can be treated *perturbatively*, i.e., the series of successive orders converges.

1.3 Electroweak Interactions

Electroweak interactions are described by the $SU(2)_L$ gauge group of weak isospin and the $U(1)_Y$ gauge group of weak hypercharge. The subscript L indicates a distinction between left- and right-handed fermions.[2] Left(right) handed fermions act as doublets(singlets) under the $SU(2)_L$ gauge group. The third component of the weak isospin, T_3, is a conserved quantum number in SM interactions. Thus from now on, "weak isospin" refers to T_3. Weak hypercharge, Y_W, is defined as $Y_W = 2(Q - T_3)$, where Q is the electric charge. Table 1.2 lists the values of T_3 for the left- and right-handed fermions (and anti-fermions). The gauge bosons associated with the $SU(2)_L$ and $U(1)_Y$ groups are the $W^0/W^\pm$ and the B respectively. The B and W^0 are rotated to give the physical (mass eigenstates) γ and Z bosons:

$$\begin{pmatrix} Z \\ \gamma \end{pmatrix} = \begin{pmatrix} \cos\theta_W & \sin\theta_W \\ -\sin\theta_W & \cos\theta_W \end{pmatrix} \begin{pmatrix} W^0 \\ B \end{pmatrix},$$

[2] A right-(left-) handed particle has its spin and momentum vector pointing in the same (opposite) direction.

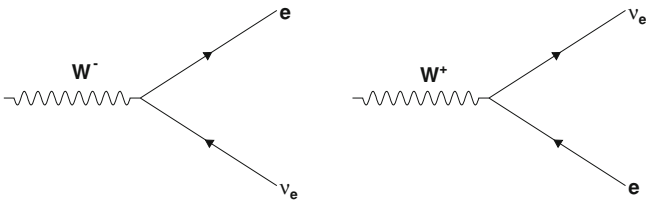

Fig. 1.2 Feynman diagrams for the decays, $W^+ \rightarrow e^+\nu_e$ and $W^- \rightarrow e^-\bar{\nu_e}$

where θ_W is the weak mixing angle that relates the coupling constants associated with the $SU(2)_L$ (g) and $U(1)_Y$ (g') gauge groups:

$$\tan\theta_W = \frac{g'}{g}.$$

This angle also relates the masses of the $W^{\pm}$ and the Z. At tree level, the SM predicts the following relation

$$\cos\theta_W = \frac{m_W}{m_Z}.$$

The masses of the W and Z boson are generated through the Higgs mechanism [6, 7]. An additional complex scalar, Higgs, field has a symmetry that is spontaneously broken at the electroweak scale. This produces additional degrees of freedom that generate gauge invariant mass terms for the W and Z whilst allowing the photon to remain massless. An additional scalar particle, the Higgs boson is also generated. The Higgs boson is the only fundamental particle in the SM that has not been observed directly in experiment, and its discovery is currently one of the main goals in the field.

The allowed charged current interactions are: the conversion of a neutrino to a charged lepton of the *same generation* or vice versa, and the conversion of an up-type quark to *any* (kinematically allowed) down-type quark or vice versa. Figure 1.2 shows Feynman diagrams for the decays, $W^+ \rightarrow e^+\nu_e$ and $W^- \rightarrow e^-\bar{\nu_e}$. The mixing between different quark flavours is governed by a unitary 3×3 matrix—the so-called Cabibbo-Kobayashi-Maskawa matrix [8, 9].

Neutral current interactions are mediated by the photon and the Z boson. The coupling constant associated with a photon-fermion vertex is eQ_f, where e is the electromagnetic coupling constant, and Q_f is the charge of the fermion. The Z boson couples to left- and right-handed fermions as

$$g^f_{(L,R)} = T^f_{3(L,R)} - Q_f \sin^2\theta_W.$$

Since the left- and right-handed fermions have different T_3 (see Table 1.2), they acquire different couplings to the Z. Traditionally, the Z-fermion coupling has been

Table 1.2 The weak isospin (T_3^f) and electric charge (Q_f) for the different fermion (f) and antifermion ($\bar{f}$) types. The three up- and down-type quarks are represented by q_u and q_d respectively. The three charged and neutral leptons are represented by q_u and q_d respectively. The subscripts L and R denote left- and right-handed fermions

Fermion	$T_{3,L}^f$ ($T_{3,L}^{\bar{f}}$)	$T_{3,R}^f$ ($T_{3,R}^{\bar{f}}$)	Q_f ($Q_{\bar{f}}$)
$\begin{pmatrix} q_u \\ q_d \end{pmatrix}$	$+\frac{1}{2}(0)$	$0(-\frac{1}{2})$	$+\frac{2}{3}(-\frac{2}{3})$
	$-\frac{1}{2}(0)$	$0(+\frac{1}{2})$	$-\frac{1}{3}(+\frac{1}{3})$
$\begin{pmatrix} l \\ \nu_l \end{pmatrix}$	$-\frac{1}{2}(0)$	$0(+\frac{1}{2})$	$+1(-1)$
	$+\frac{1}{2}(0)$	$0(-\frac{1}{2})$	$0(0)$

written in a vector minus axial-vector (V-A) form, with a vector coupling constant $c_V = g_L + g_R$ and an axial coupling constant $c_A = g_L - g_R$.

The structure of the electroweak theory has been verified to high precision at the LEP and SLC e^+e^- colliders. The Tevatron has also played an important role in discovering the top quark, and in determining the masses of the top quark and W boson. Since the SM relates the different EW parameters, it is able to predict the value of many parameters and observables, given a limited number of inputs. Figure 1.3 compares the experimental measurements of various EW observables with the SM predictions. The agreement is remarkable and consolidates the SM.

An obvious missing piece is the, as of yet, unobserved Higgs boson. The SM is able to predict the mass of the Higgs, m_H, since it introduces significant loop corrections to the masses of top-quark and the W boson as illustrated in Fig. 1.4. Figure 1.5 shows the current bounds imposed on m_H by the measurements of m_t and m_W. Currently the bounds on m_H are more limited by the precision of m_W than the precision of m_t. Thus an improved measurement of m_W is an important goal of the Tevatron and LHC experiments. Figure 1.6 compares the experimental measurements of m_W performed so far. Combination of precision electroweak data (excluding direct Higgs searches) excludes[3] $m_H > 161\,\text{GeV}$ [10]. The regions $m_H < 114\,\text{GeV}$ and $156 < m_H < 177\,\text{GeV}$ have been excluded in direct searches at LEP [11], and the Tevatron [12]. A recent combination of direct searches by the ATLAS and CMS Collaborations using up to $2.3\,\text{fb}^{-1}$ of pp collisions has excluded the region $141 < m_H < 476\,\text{GeV}$ [13]. If the SM Higgs exists in the theoretically preferred low mass region, the LHC experiments are likely to see evidence within the next year or so.

An important feature of the electroweak sector is the *non-abelian* structure of the $SU(2)_L \otimes U(1)_Y$ gauge group. This implies certain interactions between the bosons themselves. These triple-gauge-couplings play an important role in boson pair production.

[3] All exclusions that are quoted in this section are at 95 % C.L.

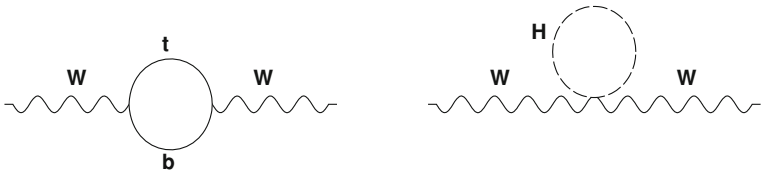

Fig. 1.3 Loop corrections to the W boson propagator from (*left*) the top quark and (*right*) the Higgs boson

Fig. 1.4 Comparison of EW measurements from experiments at LEP, SLC, and the Tevatron, with a global fit (from Ref. [14]). The *horizontal bars* indicate the number of standard deviations by which the direct measurement differs from the global fit

1.4 Strong Interactions

The strong force is described by the $SU(3)_C$ gauge group of Quantum chromodynamics (QCD), where rotations in 3-dimensional colour space are mediated by eight unitary 3×3 matrices—the Gell-Mann matrices.

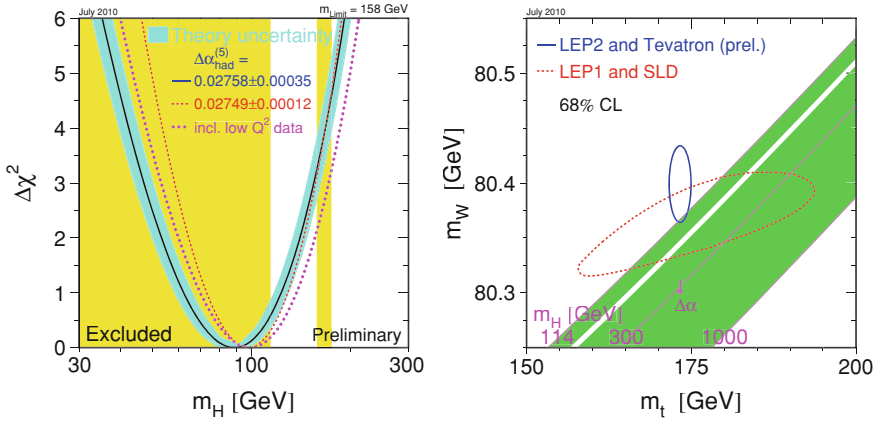

Fig. 1.5 The *left hand figure* shows the SM preferred region for m_H, where the *yellow shaded* regions are directly excluded by experimental searches. It should be noted that the direct searches from LHC have recently excluded the region $m_H > 141$ GeV [13]. The *right hand figure* shows the experimental measurement contours for m_W and m_t. The *green bands* show the SM predictions for different values of m_H. Both figures are from Ref. [14]

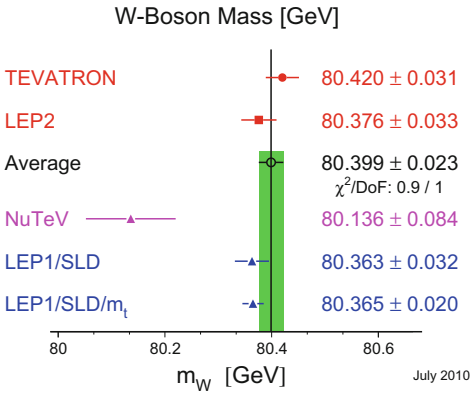

Fig. 1.6 Comparison of direct and indirect experimental measurements of m_W (from Ref. [14])

The coupling constant associated with colour exchange vertices is usually denoted g_s, though it is often more convenient to work in terms of $\alpha_s = g_s^2/4\pi$. An important feature of QCD is the running of α_s with energy scale. For n_f colours, and one-loop precision, the evolution of α_s with energy scale, Q, is given by

$$\frac{d\alpha_s}{d\log Q} = -\left(11 - \frac{2n_f}{3}\right)\frac{\alpha_s^2}{2\pi}. \tag{1.1}$$

Figure 1.7 shows various measurements of α_s at different values of energy scale. The yellow band is a prediction from QCD, calculated at four-loop precision, having

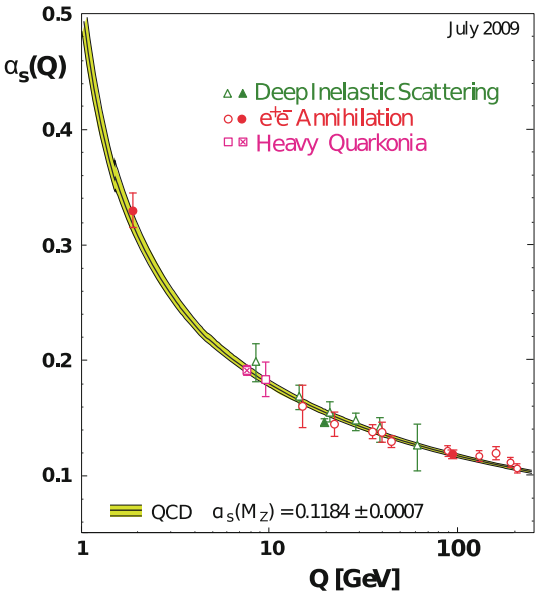

Fig. 1.7 Various measurements of α_s over a range of energy scales (from Ref. [15]). The *yellow band* is the prediction from QCD

constrained to the average of the measurements at $Q = m_Z$. It can be seen that the predicted evolution of α_s with scale agrees well with experimental observation.

At small energies (or correspondingly large distances) α_s is large, leading to the confinement of quarks to colourless hadrons; either baryons containing three quarks of different colour, or mesons containing a quark anti-quark pair of the same colour (anti-colour for the anti-quark). The confinement scale of QCD, Λ_{QCD}, is naturally around the mass of the lightest hadron (the pion) which is approximately 100 MeV.

High energy quarks and gluons (typically referred to as "partons") produced in particle scatterings readily radiate additional partons. This "showering" stops once the parton energies reach Λ_{QCD}, at which point they become confined to colourless hadrons. High energy partons therefore end up as so called "jets" of collimated hadrons.

1.5 The Drell-Yan Process

The Drell-Yan process is production of a lepton pair in hadron–hadron collisions via a virtual photon (γ^*), Z, or W [16].

1.5.1 Factorisation

At high enough energies such that α_s becomes sufficiently small (roughly 10^{-1} at electroweak scales), quark-antiquark scattering cross sections can be calculated

perturbatively. However quarks are confined to colourless hadrons which are inherently non-perturbative objects.

Luckily, calculations of hadron–hadron scattering cross sections can be *factorised* into the following general form:

$$\sigma = \sum \int_{x_a=0}^{x_a=1} \int_{x_b=0}^{x_b=1} dx_a dx_b f_a(x_a, Q^2) f_b(x_b, Q^2) \sigma_{\text{hard}}(Q^2),$$

where the sum runs over parton species, and x_a and x_b are the fractions of the parent hadron momenta carried by the interacting partons. The functions f_a and f_b are the so called parton distribution functions (PDFs), which parameterise the probability to extract a parton with a certain fraction, x, of the hadron momentum. The PDFs depend on the parton species (gluon, u-quark, d-quark etc.) and the scale of the process, Q^2. Calculation of the hard scattering cross section, σ_{hard}, can be done perturbatively. The Drell-Yan processes is special—thus far it is the only hadron–hadron scattering process for which factorisation has been demonstrated mathematically [17].

The PDFs can be constrained by various hadron–hadron and hadron–lepton scattering data over a range of x and Q^2 values. References [18] and [19] provide details on some of the most recent fits by the CTEQ and MSTW groups respectively. Extrapolation to different Q^2 values is governed by the DGLAP [20–22] equations of QCD.

1.5.2 Higher Order Corrections

Neglecting (for now at least) any intrinsic transverse motion of the partons within the hadrons, the Drell-Yan process should, at lowest order, produce a dilepton system with zero momentum transverse to the beam direction, p_T. However, at next-to-leading order in the strong coupling, an initial state quark can radiate a gluon (see right hand of Fig. 1.1), thus generating a non zero p_T. This (real correction) diagram is actually "infra-red" divergent when the radiated gluon is soft (i.e. low momentum) and/or collinear with the parent parton. The loop (virtual correction) diagram (middle of Fig. 1.1), is both "infrared" and "ultraviolet" divergent since one can integrate up to infinite loop momenta. All is not lost, since the divergences of the real and virtual diagrams actually cancel, at least when calculating the inclusive cross section [23–25].

Prediction of the p_T distribution of the dilepton system poses a problem, since, at a given order in α_s, the real and virtual diagrams populate different phase space. This results in incomplete cancellation of the divergences. leading-order (LO) in the p_T distribution only includes the left hand diagram in Fig. 1.1. Next-to-LO (NLO) includes the right hand diagram corresponding to one power of α_s, and the centre diagram corresponding to α_s^2. Although the loop diagram contains two powers of

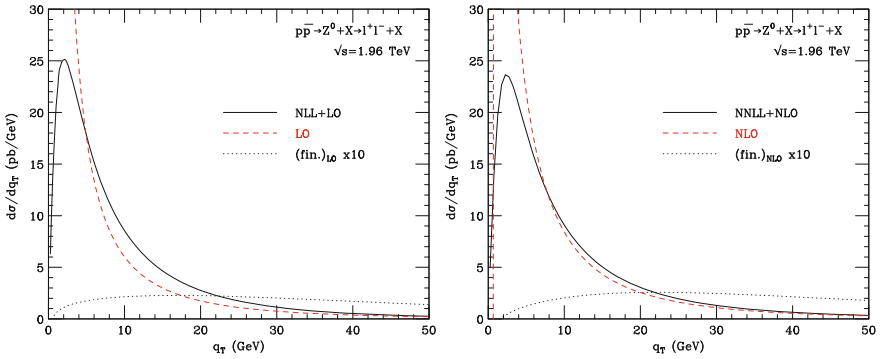

Fig. 1.8 Predictions of the Z/γ^* p_T (here given the symbol q_T) distribution from Ref. [26], up to (*left*) LO and LO+NLL, and (*right*) NLO and NLO+NNLL

α_s, it is included at NLO through interference with the L0 diagram. Figure 1.8 shows calculations from Ref. [26] of the Z/γ^* p_T distribution using different levels of accuracy. The NLO prediction is clearly divergent at low p_T. At any finite order in α_s, the coefficient of the α_s^n term contains $1/p_T^2$ multiplied by a series of logs, $\ln^m(Q/p_T)$, $m = 0, 1, .., 2n-1$. These logs become large at low p_T and spoil the convergence of the series.

A complete prescription for the Drell-Yan process at low p_T was introduced by Collins et al. [17], based on the ingredients provided by Refs. [27–31]. The expansion in powers of α_s is reorganised in terms of the logarithms, which can then be recognised as the Taylor expansion of an exponential. The large logarithms are thus exponentiated or "resummed" to all orders in α_s. This gives a finite result which can be matched[4] to fixed order calculations at larger p_T. The accuracy of the resummation depends on the order of the logs considered. Leading-log (LL) includes the (leading) $\ln^{2n-1}$ logs. Higher logarithmic accuracies include the sub-leading logs. Figure 1.8 shows that the resummation, either at next-to-LL (NLL) or next-to-NLL (NNLL), yields a finite cross section over the entire p_T range. The resummation actually needs to be performed in impact parameter ($b \sim 1/p_T$) space, such that momentum conservation in multiple parton emission can be factorised.

For $p_T < \Lambda_{\rm QCD}$, we encounter a further problem as the largeness of α_s renders QCD non-perturbative. Instead, non-perturbative (NP) functions must be determined from fits to experimental data. Various forms for the NP functions have been suggested in the literature, for example that of Brock, Landry, Nadolsky and Yuan (BLNY) [32]:

$$W(b, Q, Q_0, x_1, x_2) = \exp\left(\left[-g_1 - g_2 \ln(\frac{Q}{2Q_0}) + g_1 g_3 \ln(100 x_1 x_2)\right] b^2\right).$$

[4] The matching procedure must ensure that perturbative terms are not double counted by the fixed order and resummed calculations.

They performed a global fit to Run I Tevatron Z/γ^* data, and lower Q^2 Drell-Yan data from various fixed target experiments. Fixing $Q_0 = 1.6\,\text{GeV}$, their fit found $g_1 = 0.21^{+0.01}_{-0.01}\,\text{GeV}^2$, $g_2 = 0.68^{+0.01}_{-0.02}\,\text{GeV}^2$, and $g_3 = 0.60^{+0.05}_{-0.04}$.

The Collins-Soper-Sterman (CSS) formalism has been implemented in the MC program RESBOS[33] with the above form factor. Figure 1.9 shows the RESBOS prediction of the p_T distribution in three bins of the dilepton rapidity, y, defined as

$$y = \frac{1}{2}\ln\left(\frac{E + p_z}{E - p_z}\right),$$

where E is the dilepton energy, and p_z is the dilepton momentum along the beam direction. For Z/γ^* production at the Tevatron, $Q \sim 90\,\text{GeV}$, and $x_1, x_2 \sim 10^{-3} - 10^{-1}$. In this case, the p_T distribution is most sensitive to the g_2 parameter, as can be seen in Fig. 1.9—a larger value of g_2 corresponds to a broader p_T distribution.

A particularly interesting part of the NP form factor is the x dependence. Semi inclusive deep inelastic scattering data from HERA [34, 35] indicates a broadening of the form factor at low values of x [36]. For Z/γ^* production at the Tevatron, the boson rapidity is related to the x of the two partons:

$$x_{1,2} = \frac{Q}{\sqrt{s}} e^{\pm y},$$

where $\sqrt{s}$ is the hadron–hadron centre of mass energy of the collider. Large values of boson rapidity correspond to one parton with small x and one parton with large x. The "small-x broadening" [36] would widen the predicted p_T distribution at large values of $|y|$, as shown in Fig. 1.9. The effect becomes significant for $|y| > 2$, corresponding to one parton with $x < 10^{-2}$. At the LHC, *inclusive* production of W, Z, and Higgs bosons involves partons with similarly small values of x. The small-x broadening would therefore have a dramatic effect on the p_T spectra in these processes at the LHC [37]. Early measurements from the ATLAS [38] and CMS [39] are in reasonable agreement with predictions that do not include such effects.

1.5.3 Monte Carlo Event Generators

Much of the hadron collider physics analysis program relies on Monte Carlo event generators to predict kinematic distributions and rates for signal and background processes. So far, the state-of-the-art resummation programs (e.g. RESBOS) have only been able to predict distributions for the final state leptons, rather than the full particle content.

The programs PYTHIA [40] and HERWIG++ [41] match leading-order (LO) matrix elements to leading-log (LL) parton showers, which evolve high energy partons down to some predefined cut-off scale by radiating additional partons. Models for